Article

Magnetic Anisotropy Tailoring by 5d Doping in $(Fe,Co)_5SiB_2$ Alloys

Diana Benea *

Posted Date: 7 November 2023

doi: 10.20944/preprints202311.0425.v1

Keywords: ab-initio calculations; magneto-crystalline anisotropy; magnetization; rare earth free magnets

Article

Magnetic Anisotropy Tailoring by 5d Doping in $(Fe,Co)_5SiB_2$ Alloys

Diana Benea

Faculty of Physics, Babes-Bolyai University Cluj-Napoca, Kogalniceanu 1 str., 400084 Cluj-Napoca, Romania; diana.benea@ubbcluj.ro

Abstract: Band structure calculations using the spin-polarized relativistic Korringa-Kohn-Rostoker (SPRKKR) band structure method have been performed to determine the intrinsic magnetic properties (magnetic moments, magneto-crystalline anisotropy -MAE and Curie temperatures) of the $Fe_{5-x-y}Co_xM_ySiB_2$ (M = Re, W) alloys. The general gradient approximation for exchange-correlation potential and the atomic sphere approximation (GGA ASA) have been employed. Previous studies showed that the Co doping is turning the in-plane into axial anisotropy for a certain doping range, whilst the 5d doping enables a strong spin-orbit coupling of Fe-3d and M-5d states which is needed to enhance the MAE. The theoretical calculations aim to find the dependence of the anisotropy constant K_1 for combined Co and M doping, building a two-dimensional (2D) map of K_1 for $0 \le x \le 2$ and $0 \le y \le 1$. Similar theoretical 2D maps for magnetization and Curie temperature vs. Co and M content (M = W and Re) have been built, allowing to select alloy compositions with enhanced values of uniaxial anisotropy, magnetization and Curie temperature. Magnetic properties of $Fe_{4.1}W_{0.9}SiB_2$ alloy that meets the selection criteria for axial anisotropy $K_1 > 0.2$ meV/f.u., Curie temperature $T_c > 800$ K determined by mean field approach and magnetization $\mu_0 M_s > 1$ T are discussed.

Keywords: ab-initio calculations; magneto-crystalline anisotropy; magnetization; rare earth free magnets

1. Introduction

Magnetic materials are crucial for technological development in many sectors, such as electric motors, transformers, power generators or recording media. High performance permanent magnets with large saturation magnetization, high Curie temperature and large uniaxial magnetic anisotropy are necessary, these requirements being currently fulfilled by the rare earth permanent magnets such as Sm-Co and Nd-Fe-B [1]. The volatile prices and restricted accessibility to the rare earth resources raised a strategic issue, directing the research efforts in the last two decades to the search of new magnetic materials with close performance to Sm-Co and Nd-Fe-B magnets, but with lower rare earth content. Also, the search for new permanent magnets without rare earth elements arouse interest in the magnetic materials research [2–4]. Due to their reduced costs and small supply risks, their use in less-demanding applications can be efficient. This research direction is motivated by the large gap in the price-performance diagram between the hard ferrite/Alnico magnets and the high performant RE which could be filled in by new rare-earth free permanent magnets. In this last category, the Fe compounds with anisotropic crystal structure are important candidates for functional rare-earth free permanent magnets due to their lower price, standardized preparation procedure and good mechanical properties. Such compound is Fe_5SiB_2 discovered in the 1960's by Aronsson et al. [5], having a Cr_5B_3 structure type (*I4/mcm* space group). According to the recent research, a saturation magnetization of 9.2 μ_B/f.u. has been theoretically predicted for this compound [6], whilst the magnetic measurements at 10 K show a value of 1.1 MA/m, with large values of Fe spin magnetic moments on both Fe crystal sites (2.31 μ_B for Fe on *4c* site and 2.10 μ_B for Fe on *16l* site) determined by neutron diffraction at 16 K [7]. A magnetic anisotropy constant K_1 of -0.28 MJ/m^3 [6] and

Preprints (www.preprints.org) | NOT PEER-REVIEWED | Posted: 7 November 2023 doi:10.20944/preprints202311.0425.v1

experimentally determined Curie temperature over 800 K [7,8] have been also reported for this compound. The in-plane anisotropy and the spin reorientation at ~ 170 K [7] makes this compound inefficient for permanent magnets (PM) development, but further research found that the Co for Fe substitution in $(Fe,Co)_5SiB_2$ is able to turn the sign of MAE from negative to positive, enabling an axial easy magnetization direction for the corresponding alloys, as well as the decrease of the spin reorientation transition temperature down to the lowest temperature [9]. Previous studies showed that doping with *5d* elements (M) is effective by building stronger uniaxial anisotropy in Fe alloys, due to the stronger spin-orbit coupling of Fe-*3d* and M-*5d* states. Earlier research on Fe_5PB_2 doped with W of Thakur et al. [10] showed that the anisotropy constant K_1 increases from 0.152 MJ/m^3 in Fe_5PB_2 to 1.135 MJ/m3 in Fe_4WPB_2, this enhancement being attributed to the strong spin-orbit coupling of Fe-3d states and W-5d states. Still, *5d* doping could decrease the magnetization and the Curie temperature in Fe alloys, the doping amount in this case having to be optimized to maintain them at values compatible with functional applications. Our previous theoretical investigations showed for Fe_4WSiB_2 alloy an increased anisotropy constant of 0.218 meV/f.u. but lower total magnetic moment (7.97 μ_B/f.u.) and Curie temperature (747 K) compared with the undoped Fe_5SiB_2 compound [11]

Also, other *5d* elements could be effective for the magnetic anisotropy tailoring. For instance, *5d* doping in Fe_2B alloy showed larger efficiency for Re doping (K_1 = 1.5 MJ/m^3, magnetization $\mu_0 M_s$ = 1.22 T and estimated Curie temperature of 595 K for $Fe_{1.52}Re_{0.48}B$), whilst the W doping effects on anisotropy are much weaker [12].

In this study, we present the magnetic anisotropy behaviour by *5d* doping in the $Fe_{5-x-y}Co_xM_ySiB_2$ alloys (M = W and Re) in the range $0 \le x \le 2$ and $0 \le y \le 1$. Two-dimensional 2D maps of the anisotropy constant are built, allowing to select the composition range for compounds with large uniaxial anisotropies. Further investigations on the magnetization and Curie temperature behaviour vs. Co and M content (M = W and Re) enables a detailed view on the intrinsic magnetic properties of these alloys. Fully relativistic theoretical calculations done in the framework of density functional theory (DFT) using the exchange-correlation potential under general gradient approximation with the Perdew et al. (PBE) parametrization [13] were employed for the current investigations.

2. Results and Discussions

2.1. Crystal Structure

The crystal structure of the $Fe_{5-x-y}Co_xM_ySiB_2$ alloys (Figure 1) consists of a body-centered tetragonal unit cell (space group I4/mcm, no. 140), with Fe atoms on two different sites (4c and 16l), the B atoms on 8h sites, whilst Si atoms occupy the 4a crystallographic sites. The lattice parameters determined by X-ray diffraction are a = 5.5541 Å and c = 10.3429 Å [7].

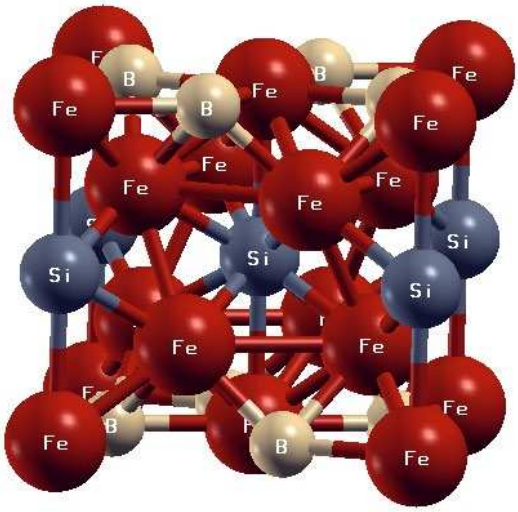

Preprints (www.preprints.org) | NOT PEER-REVIEWED | Posted: 7 November 2023 doi:10.20944/preprints202311.0425.v1

Figure 1. The body-centered tetragonal unit cell (space group I4/mcm, no. 140) of Fe_5SiB_2 alloy, with Fe atoms on two different sites (4c and 16l), the B atoms on 8h sites and Si atoms on 4a crystallographic sites. Graphic program XCrySDen [15] was used.

The electronic band structure calculations for the $Fe_{5-x-y}Co_xM_ySiB_2$ alloys (for $0 \le x \le 2$ and $0 \le y \le 1$) in tetragonal structure (space group I4/mcm) using the experimental lattice parameters [2,14] have been performed. The experimental free parameters of 8h and 16l crystallographic sites determined by Cedervall et al. for Fe_5SiB_2 have been considered [7]. The lattice constants of the W and Re-doped alloys have been evaluated using the lattice constants of Re_5SiB_2, W_5SiB_2 and Co_5SiB_2 [7,14] and considering their linear dependence by doping. The occupation of Co atoms on 16l crystal sites has been considered, according to our previous investigations [8]. Similar preferential occupation has been obtained for Re atoms, whilst a random occupation of the 4c and 16l sites has been derived for W atoms by total energy calculations.

2.2. Magnetic Moments

The band structure calculations for Fe_5SiB_2 alloy have been performed using different exchange and correlation parametrizations (local density approximation LDA, as well as GGA) within atomic spheres approximation as well as the full potential approach. The results of the calculations are listed in Table 1 together with the results of experimental measurements [7] and with other theoretical results [6].

Table 1. Total magnetic moments and site-dependent spin and orbital magnetic moments for Fe_5SiB_2 alloy, determined by different exchange-correlation approaches in the ASA and full potential mode. The experimental values for saturation magnetization and neutron diffraction [7,6] are also shown.

	SPR-KKR						**FPLO** [6]		**Neutron diffraction**
	VWN-ASA		GGA-ASA		GGA-FP		GGA-FP		[7]
	$m_s(\mu_B)$	$m_l(\mu_B)$	$m_s(\mu_B)$	$m_l(\mu_B)$	$m_s(\mu_B)$	$m_l(\mu_B)$	$m_s(\mu_B)$	$m_l(\mu_B)$	$m_{tot}(\mu_B)$
Fe *4c*	2.20	0.05	2.35	0.05	2.08	0.05	2.24	0.05	2.31
Fe *16 l*	1.61	0.04	1.81	0.04	1.88	0.04	1.87	0.04	2.10
Si *4a*	-0.14	-	-0.17	-	-0.16	-	-0.25	-	-
B *8h*	-0.13	-	-0.15	-	-0.14	-	-0.25	-	-
Total (μ_B/f.u.)	8.25	0.21	9.12	0.22	9.19	0.22	8.98	0.22	10.71
	8.46		9.34		9.41		9.20		
Exp. $M_s(\mu_B$/f.u.) [7]					9.35				

According to our calculations, the Fe_5SiB_2 alloy is ferromagnetic with a total magnetic moment between 8.46 and 9.41 μ_B/f.u., depending significantly on the exchange-correlation potential and on the potential symmetry (spherical in ASA and no shape approximation in full potential approach). As can be seen in Table 1, the VWN-ASA approach gives an underestimated total magnetic moment compared with the experimental data. Better agreement is obtained by the use of the GGA approach, with total magnetic moment of 9.34 μ_B/f.u. (GGA-ASA) and 9.41 μ_B/f.u. (GGA-FP). Also, the SPR-KKR shows similar values of individual magnetic moments with FPLO calculations, with only minor deviation determined most probably by the lattice constants used for calculations. The Fe magnetic moments show higher values for Fe 4c, but the ratio between Fe 4c/16l moments depend on the calculation approach.

Based on these results, the GGA-ASA calculation mode has been chosen to deal with the combined Co and M (M = Re, W) doping. Moreover, the GGA-ASA calculated value of $\mu_0 M_s$ (1.36T) is close to the value determined experimentally by McGuire et al. (1.31 T) [9].

The total magnetic moments calculated for the $Fe_{5-x-y}Co_xM_ySiB_2$ alloys for $0 \le x \le 2$ and $0 \le y \le 1$ are used to build a two-dimensional map of magnetization vs. Co and M content (x,y), shown in Figure 2. According to the contour maps for several selected values of total magnetic moment, the Re and W doping have similar effect in combination with Co doping on the magnetization of the Fe_{5-x-}

Preprints (www.preprints.org) | NOT PEER-REVIEWED | Posted: 7 November 2023 doi:10.20944/preprints202311.0425.v1

$_y$Co$_x$M$_y$SiB$_2$ alloys. The values of magnetization decrease by both combined doping (Co and Re; Co and W, respectively) from 9.34 μ_B/f.u. to values lower than 5 μ_B/f.u. The decrease of magnetization was evidenced already for doping with Co [6, 8]. Still, the use of combined doping (Co + Re; Co + W) is able to enhance this tendency, as shown in Figure 2. If the desired values of magnetization are set to values over 6 μB/f.u., the corresponding alloys have Co content x ≤ 1.5 and M content y ≤ 0.6.

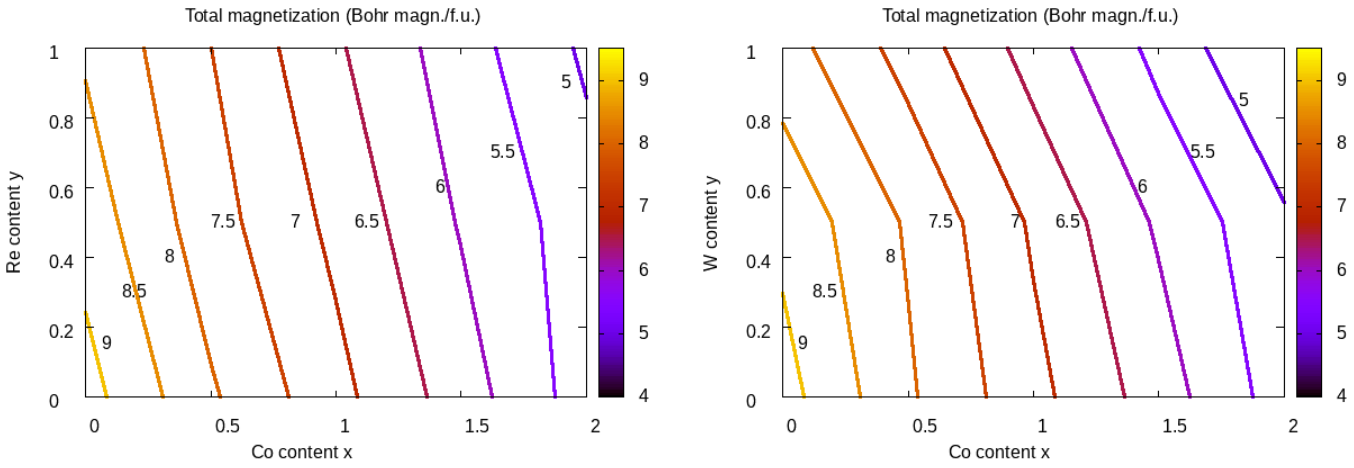

(**a**) (**b**)

Figure 2. The calculated total magnetization for the Fe$_{5-x-y}$Co$_x$M$_y$SiB$_2$ alloys for M = Re (**a**) and M = W (**b**) represented as a 2D map vs. Co and M content (x, y). The isolines for discrete values of magnetization (in μ_B/f.u.) are shown.

2.3. Magnetic Anisotropy

The earlier reports show that the anisotropy constant of (Fe,Co)$_5$SiB$_2$ alloys is changing the sign for a certain range of Co amount [6,8]. This effect is accounted in the present study, as an easy-axis anisotropy is obtained by Co doping, followed by expected anisotropy enhancement by further doping with *5d* elements. The validity of this mechanism is discussed in the following, using the representation of the anisotropy constants K_1 calculated for Fe$_{5-x-y}$Co$_x$M$_y$SiB$_2$ alloys. The K_1 values obtained for both M = Re, and W in a 5x3 grid for $0 \le x \le 2$ and $0 \le y \le 1$ ($\Delta x = \Delta y = 0.5$) have been used to build the $K_1(x,y)$ 2D maps. The K_1 isolines between -0.3 meV/f.u and 0.25 meV/f.u. have been evidenced in Fig.3. As can be seen, much different K_1 2D maps have been obtained by Re/W doping in Fe$_{5-x-y}$Co$_x$M$_y$SiB$_2$ alloys. In the case of Re, values of K_1 over 0.25 meV/f.u. can be obtained for a combination of Co doping with approx. $x \ge 1.8$ and Re doping with $y \ge 0.7$. The disadvantage of the Re doping is visible by overlapping the M_s 2D map (Figure 2) and K_1 2D map (Figure 3). The (x,y) areas with large K_1 values almost overlap with the areas with low magnetization values, as $M_s < 5$ μ_B/f.u. for $x \ge 1.5$. This behaviour of magnocrystalline anisotropy is opposite to that evidenced in Fe$_2$B alloy, where Re doping promoted large axial anisotropy [12].

Preprints (www.preprints.org) | NOT PEER-REVIEWED | Posted: 7 November 2023 doi:10.20944/preprints202311.0425.v1

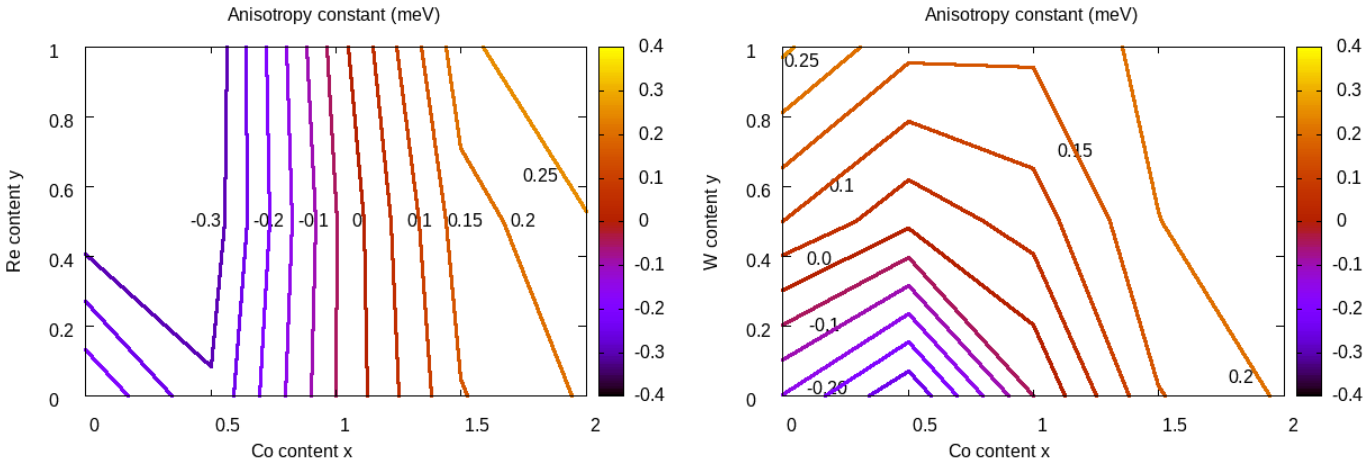

(**a**) (**b**)

Figure 3. The calculated anisotropy constants for the $Fe_{5-x-y}Co_xM_ySiB_2$ alloys for (**a**) M = Re and (**b**) M = W represented as a 2D map vs. Co and M content (x, y). The isolines for discrete values of K_1 (in meV) are shown.

On the other hand, W doping can increase the anisotropy of the Fe_5SiB_2 alloy, values of $K_1 \geq 0.2$ meV/f.u. being obtained for x = 0 and y > 0.8. Also, values of $K_1 \geq 0.25$ meV/f.u. are seen for x = 0 and y ~ 1. By overlapping the 2D maps of M_s and K_1 in the case of M = W, one can find magnetization values between 8 - 8.5 μ_B/f.u. It is interesting to note that in the case of Re doping, the area (x = 0, y > 0.9) corresponds to largest value of in-plane magnetocrystalline anisotropy, whilst W doping alone is able to switch the anisotropy to easy-axis, without additional Co doping.

2.4. Curie Temperatures and Exchange-Coupling Parameters

The Curie temperatures (T_c) have been determined by mean field approach (MFA) using the procedure described in Section 3. The grid data for T_c have been used to build isolines with constant values of T_c, which are represented in Figure 4. According to our calculations, Fe_5SiB_2 alloy is ferromagnetic with a Curie temperature of 1162 K calculated by mean field approach. As the mean field method is known to overestimate by ~20% the Curie temperature values, the estimated T_c would be comparable with the experimental value of 850 K [8].

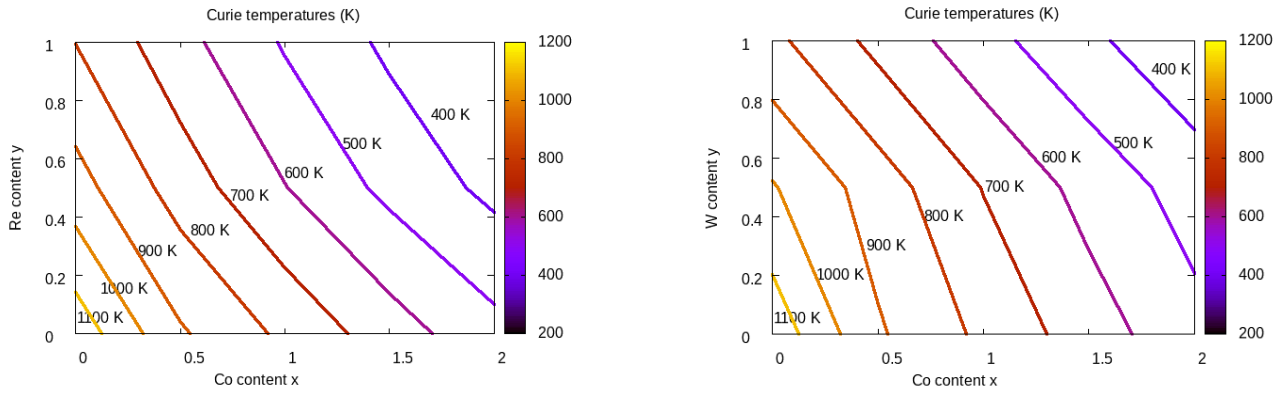

(**a**) (**b**)

Figure 4. The calculated Curie temperatures for the $Fe_{5-x-y}Co_xM_ySiB_2$ alloys for (**a**) M = Re and (**b**) M = W represented as a 2D map vs. Co and M content (x, y). The isolines for discrete values of Tc (in K) are shown.

Preprints (www.preprints.org) | NOT PEER-REVIEWED | Posted: 7 November 2023 doi:10.20944/preprints202311.0425.v1

From the T_c representation in Figure 4, it is obvious that the combined Co + M doping is going to decrease the Curie temperatures for both M = Re and W. This decrease is slightly steeper in the case of Co + Re. For Re-doped alloys, by overlapping the areas with $K_1 \geq 0.2$ meV/f.u. of the K_1 2D map to the Curie temperatures map, the corresponding alloys have T_c values under 400 K, which makes the Re-doping rather unsuited for PM applications.

On the other hand, the expected T_c values of the W-doped alloys with anisotropy constant $K_1 \geq 0.2$ meV/f.u. (obtained for x = 0 and y > 0.8) are between 850 – 900 K, compatible with PM applications.

Due to the promising intrinsic properties $Fe_{1-y}W_ySiB_2$ alloys in doping range y > 0.8, we investigated into more details the magnetic properties of such W-doped alloy. We used a complementary approach by considering particular microscopic models making use of magnetic interaction based on the classical Heisenberg Hamiltonian described in Section 3. Using this approach, the Fe-Fe exchange-coupling parameters are obtained and represented as a function of distance (in units of lattice constant a). The Fe-Fe exchange interaction for Fe_5SiB_2 and $Fe_{4.1}W_{0.9}SiB_2$ alloys are presented in Figure 5. As can be seen in Figure 5, the dominant exchange interactions are positive, favouring the ferromagnetic ordering. Negative exchange interactions are also seen, mostly between Fe *16l* spins at distances of between 0.6a and 0.9a. The largest exchange interactions are between Fe *4c* - Fe *16l* nearest neighbours. These exchange interactions are affected by the W doping and a decrease between the nearest neighbour's exchange-coupling parameters in $Fe_{4.1}W_{0.9}SiB_2$ compared with Fe_5SiB_2 can be seen. Also, a decrease of the exchange coupling parameters values by W doping is observed for the interactions between the Fe *4c* - Fe *4c* spins. The exchange interactions between nearest Fe *4c* - Fe *4c* spins are much smaller, as their interatomic distance are considerably larger than those of the other pairs. The Curie temperature is mostly determined by the Fe *16l* - Fe *16l* and Fe *4c* - Fe *16l* exchange interactions.

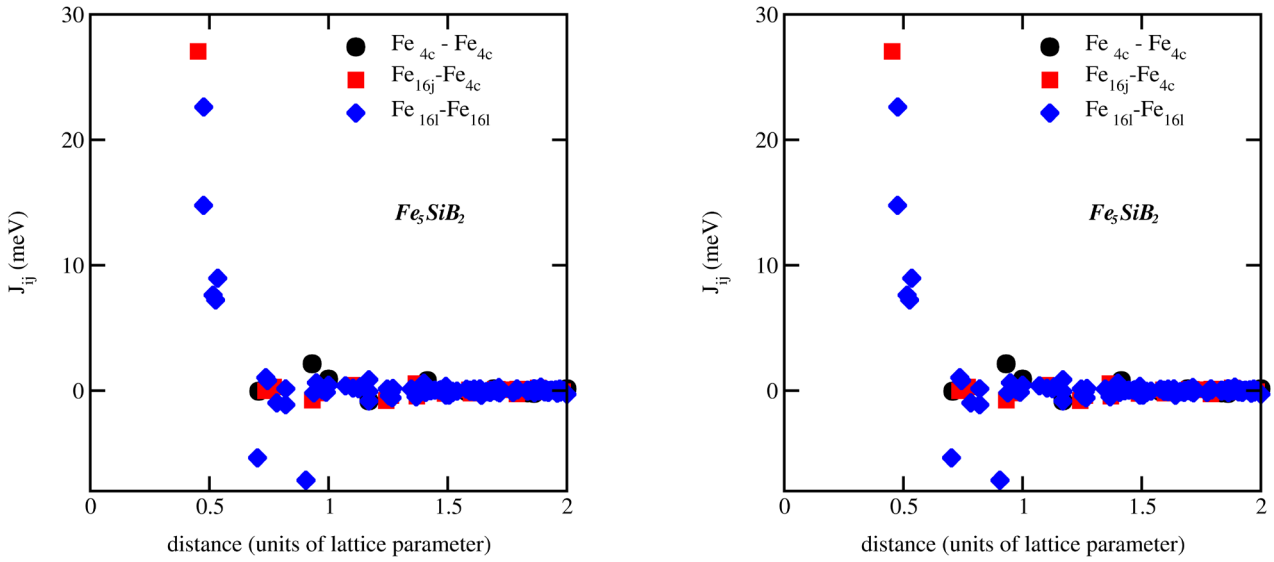

Figure 5. Fe-Fe exchange coupling parameters for (**a**) Fe_5SiB_2 and (**b**) $Fe_{4.1}W_{0.9}SiB_2$ alloys plotted as a function of distance between Fe spins.

The spin and orbital magnetic moments, magnetization $\mu_0 M_s$, anisotropy constant K_1, Curie temperature and hardness parameter for $Fe_{4.1}W_{0.9}SiB_2$ alloy are listed in Table 2. In particular, the spin and orbital moments on Fe sites (2.43 μ_B and 0.07 μ_B for Fe *4c*; 1.95 μ_B and 0.06 μ_B for Fe *16l*) and are higher compared with the corresponding values in Fe_5SiB_2 (see Table 1) but the weight of the magnetic atoms decreases with about 18 %, resulting in a magnetization decrease (8.37 μ_B/f.u.) by W doping, which correspond to a $\mu_0 M_s$ value of 1.17 T.

Preprints (www.preprints.org) | NOT PEER-REVIEWED | Posted: 7 November 2023 doi:10.20944/preprints202311.0425.v1

Table 2. Spin and orbital magnetic moments, magnetization $\mu_0 M_s$ together with the magnetocrystalline anisotropy constant K_1 and Curie temperature for the $Fe_{4.1}W_{0.9}SiB_2$ alloy.

	lattice const. *a,c* (Å)	m_s (μ_B/f.u.)	m_l (μ_B/f.u.)	$\mu_0 M_s$ (T)	K_1 (meV/f.u.)	K_1 (MJ/m3)	κ	Tc (K)
$Fe_{4.1}W_{0.9}SiB_2$	5.64; 10.47	8.14	0.23	1.17	0.24	0.46	0.65	863

The results from Table 2 show that $Fe_{4.1}W_{0.9}SiB_2$ alloy is a semihard permanent magnet, with $\mu_0 M_s > 1$T and magnetic anisotropy energy of 0.46 MJ/m^3, close to the values in Sr-ferrite [4]. The magnetic hardness parameter captures the potential of the present alloy with adequate magnetization M_s (1.17 T) to be developed into a compact permanent. The value obtained according to formula $\kappa = \sqrt{K_1/\mu_0 M_s^2}$ is 0.65, corresponding to a semi-hard magnetic material. The Curie temperature is expected to be overestimated by MFA, but a value over 680 K is still expected for the $Fe_{4.1}W_{0.9}SiB_2$ alloy. The high value of Curie temperature allows the use of this alloys for relative high temperature applications.

3. Materials and Methods

Spin-polarized fully relativistic band structure calculations based on the Korringa-Kohn-Rostoker (SPRKKR) method has been used for theoretical calculations [16]. This calculation method is based on the KKR Green's function formalism that makes use of the multiple scattering theory. Within this approach, the so-called t-scattering matrices describing the scattering properties of each scattering centre (atom) are determined. In the second step, the multiple scattering matrices by all atoms in the lattice are calculated accounting that that the incident wave at each atom is the sum of the outgoing waves from all other atoms. The central role in the KKR Green's function method is played by the crystal Green's function, which is efficiently related to the Green's function of free space via the Dyson equation. The SPR-KKR calculation method supplies all the information about the electronic structure, similar to other band structure methods which are using the energy eigenvalues and eigenfunctions to represent the electronic structure. In addition, the SPR-KKR band structure method has an important advantage by dealing with chemical disorder, as the coherent potential approximation (CPA) [17] was efficiently integrated by defining a Green's function of average crystal medium, which is determined self-consistently through the condition that the concentration average of the various atom types should not produce any additional scattering in this medium [17]. In this way, the SPR-KKR is a more efficient and reliable alternative to more tedious supercell techniques, requiring enlarged unit cells and atomic configuration averaging in the supercells in order to describe the alloys properties. More details about the SPR-KKR method are extensively described elsewhere [16].

The local spin density approximation (LSDA) [18], as well as the generalized gradient approximation with the parametrization of Perdew et al. (GGA-PBE) [13] have been used to account on the exchange and correlation effects. The k-space integration was performed using the special points method [19]. The study of the magnetic anisotropy has been performed by magnetic torque calculations. The magnetic torque acting on the magnetic moment $\overrightarrow{\mathbf{m}_i}$ of the atomic site *i*, oriented along the magnetization direction $\overrightarrow{\boldsymbol{M}}$ generates a component $\boldsymbol{T_{\hat{u}}(\theta,\varphi) = -\partial E(\overrightarrow{M}(\theta,\varphi))/\partial\theta}$ with respect to axis $\hat{\boldsymbol{u}}$, where θ and φ are the polar angles [20,21]. The magnetic anisotropy energy, defined as the energy difference between the in-plane and out-of-plane magnetization directions and the magnetic torque are related by a special geometry. By setting the polar angles to $\theta = \pi/4$ and $\varphi = 0$, the calculated magnetic torque is $\boldsymbol{T_{\hat{u}}(\pi/4, 0) = E_{[100]} - E_{[001]}}$ [21].

The magnetic behaviour of the $Fe_{5-x-y}Co_xM_ySiB_2$ alloys is investigated by a complementary approach based on the classical Heisenberg Hamiltonian described by the expression:

$$\boldsymbol{H_{ex} = -\sum_{i,j} J_{ij}\hat{e}_i \cdot \hat{e}_j} \quad (1)$$

 doi:10.20944/preprints202311.0425.v1

where the summation is performed on all lattice sites i and j and $\hat{\boldsymbol{e}}_{\boldsymbol{i}}$, $\hat{\boldsymbol{e}}_{\boldsymbol{j}}$ are the unit vectors of magnetic moments on sites i and j, respectively. The total energy difference $\Delta \boldsymbol{E}_{\boldsymbol{ij}}$ due to infinitesimal change in angle between magnetic moments of (i, j) spin pair has been calculated in scalar-relativistic mode and expressed to lowest order with respect of the orientation angle between $\hat{\boldsymbol{e}}_{\boldsymbol{i}}$ and $\hat{\boldsymbol{e}}_{\boldsymbol{j}}$. Using the expression derived by Liechtenstein [20] based on the magnetic force theorem, a one-to-one mapping between the exchange-coupling energy $\Delta \boldsymbol{E}_{\boldsymbol{ij}}$ and the Heisenberg Hamiltonian is obtained, allowing to determine the J_{ij} exchange coupling parameters. The J_{ij} exchange coupling parameters have been calculated for all magnetic atoms as a function of distance up to 15 Å around each lattice site. The mean field approach has been used to derive the Curie temperatures, using the calculated J_{ij} exchange coupling parameters, according to the expression [20,22]:

$$\boldsymbol{T}_{\boldsymbol{c}}^{\boldsymbol{rough-MFA}} = \frac{\boldsymbol{2}}{\boldsymbol{3k_B}} \sum_{\boldsymbol{i}} \boldsymbol{J_{0i}} \tag{2}$$

where $\boldsymbol{J_{0i}}$ is the exchange-coupling parameters i^{th} site sum over all coordination shells.

4. Conclusions

The present research aims to find the M *5d* doping elements and their amount able to switch to the easy-axis anisotropy and to enhance it by enabling a strong spin-orbit coupling between the Fe-*3d* and M-*5d* states. Theoretical studies on the $Fe_{5-x-y}Co_yW_xSiB_2$ alloys show the decrease of total magnetic moment and Curie temperatures of the alloys by increasing W and Re content x. Also, the theoretical calculated anisotropy constant turns from planar for Fe_5SiB_2 alloy to axial for $Fe_{5-x-y}Co_yW_xSiB_2$ in different zones of the 2D map, showing rather opposite impact of Re/W doping on the magnetocrystalline anisotropy behaviour in these alloys. The superposition of the 2D maps for magnetization, MAE and Curie temperatures allowed us to conclude that W doping is favourable for development of intrinsic properties compatible with PM applications, even without Co doping. In the case of Re + Co doping, such concentrations range was not found, due to the reversed effects of combined doping on the magnetization and Curie temperature on one side and magnetocristalline anisotropy, on the other side. Despite of its strong spin-orbit coupling with Fe-*3d* states, the Re doping determined large anisotropy constants for the alloys having low Curie temperatures and magnetizations, incompatible with PM applications. On the other hand, the W-doped Fe_5SiB_2 alloys can be optimized in order to allow its use as semi-hard magnet in nanocomposite magnetic materials.

Funding: This research was funded by Romanian Ministry of Education and Romanian Ministry of Research and Innovation, CCCDI-UEFISCDI grant PN-III-P2-2.1-PED-2019-3484.

Data Availability Statement: Data are available on request.

Conflicts of Interest: The authors declare no conflict of interest. The funders had no role in the design of the study; in the collection, analyses, or interpretation of data; in the writing of the manuscript; or in the decision to publish the results.

References

1. Coey: J.M.D.; Perspective and Prospects for Rare Earth Permanent Magnets, *Engineering* **2020** 6 119-131. https://doi.org/10.1016/j.eng.2018.11.034
2. Mohapatra, J; Liu, J. P.; Rare-Earth-Free Permanent Magnets: The Past and Future. In *Handbook of Magnetic Materials* ed. Elsevier **2018** 27 1-57. https://doi.org/10.1016/bs.hmm.2018.08.001
3. Skokov, K. P.; Gutfleisch, O.; Heavy rare earth free, free rare earth and rare earth free magnets - Vision and reality, *Scripta Mater.* **2018** 154 289-294. https://doi.org/10.1016/j.scriptamat.2018.01.032
4. Cui, J; Kramer, M; Zhou, L; et al, Current progress and future challenges in rare-earth-free permanent magnets, *Acta Mater.* **2018** 158 118-137. https://doi.org/10.1016/j.actamat.2018.07.049
5. Aronsson, B.; Engström, I.; X-ray Investigations on Me-Si-B Systems (Me = Mn, Fe, Co). *Acta Chem. Scand*, **1960** 14 1403.
6. Werwiński, M.; Kontos, S.; Gunnarsson, K.; Svedlindh, P.; Cedervall, J.; Höglin, V.; Sahlberg, M.; Edström, A.; Eriksson, O.; Rusz, J.; Magnetic properties of Fe_5SiB_2 and its alloys with P, S, and Co, *Phys. Rev B* **2016** 93 174412. https://doi.org/10.1103/PhysRevB.93.174412

7. Cedervall,J.; Kontos, S.; Hansen, T. C.; Balmes, O.; Martinez-Casado, F. J.; Matej, Z.; Beran, P.; Svedlindh, P.; Gunnarsson, K.; Sahlberg, M.; *J. Solid State Chem.* **2016** 235 113-118. https://doi.org/10.1016/j.jssc.2015.12.016
8. Hirian, R.; Isnard, O.; Pop, V.; Benea, D.; Investigations on the magnetic properties of the $Fe_{5-x}Co_xSiB_2$ alloys by experimental and band structure calculation methods, *J. Magn. Magn. Mater.* **2020** 505 166748. https://doi.org/10.1016/j.jmmm.2020.166748
9. McGuire, M.A.; Parker, D.S.; Magnetic and structural properties of ferromagnetic Fe_5PB_2 and Fe_5SiB_2 and effects of Co and Mn substitutions, *J. Appl. Phys.* **2015** 118 163903 https://doi.org/10.1063/1.4934496
10. Thakur, J.; Rani, P.; Tomar, M.; Gupta. V.; Kashyap, M. K.; Enhancement of magnetic anisotropy of Fe_5PB_2 with W substitution: ab-initio study, *AIP Conf. Proc*. **2019** 2093, 020012. https://doi.org/10.1063/1.5097081
11. Hirian, R.; Pop, V.; Isnard, O.; Benea, D.; Magnetic properties of the (Fe,Co)5SiB2 alloys by W doping, *Studia UBB Physica* **2022** 67 1.
12. Benea, D.; Pop, V.; Magnetic Properties of the Fe_2B Alloy Doped with Transition Metal Elements, *Magnetochemistry* **2023** 9, 109. https://doi.org/10.3390/magnetochemistry9040109
13. Perdew, J.P.; Burke, K.; Ernzerhof, M., Generalized Gradient Approximation Made Simple, Phys. Rev. Lett. 1996 77 3865. https://doi.org/10.1103/PhysRevLett.77.3865
14. Pan, Y.; Guan, W. M.; Exploring the structural stability and mechanical properties of TM5SiB2 ternary silicides, *Ceramics International* **2018** 44 9893 https://doi.org/10.1016/j.ceramint.2018.03.005
15. Kokalj, A.; XCrySDen—a new program for displaying crystalline structures and electron densities, *J. Mol. Graphics Modelling*, **1999**, 17, 176-179. https://doi.org/10.1016/S1093-3263(99)00028-5
16. Ebert H.; Ködderitzsch, D.; Minar, J., Calculating condensed matter properties using the KKR-Green's function method—recent developments and applications, Rep. Prog. Phys. 2011 74 096501. https://doi.org/10.1088/0034-4885/74/9/096501
17. Faulkner, J. S.; Stocks, G.M., Calculating properties with the coherent-potential approximation, Phys. Rev. B 1980 21 3222. https://doi.org/10.1103/PhysRevB.21.3222
18. Vosko, S. H.; Wilk, L.; Nusair, M.; Accurate spin-dependent electron liquid correlation energies for local spin density calculations: a critical analysis, *Can. J. Phys*. **1980** 58 1200. https://doi.org/10.1139/p80-159
19. Monkhorst, H.; Pack, J. Special points for Brillouin-zone integrations, Phys. Rev. B 1976 13, 5188. https://doi.org/10.1103/PhysRevB.13.5188
20. Liechtenstein, A. I.; Katsnelson, M. I.; Antropov, V. P.; Gubanov, V. A., Local spin density functional approach to the theory of exchange interactions in ferromagnetic metals and alloys, J. Magn. Magn. Mater. 1987 67 65-74. https://doi.org/10.1016/0304-8853(87)90721-9
21. Mankovsky, S.; Polesya, S.; Minar, J.; Hoffmann, F.; Back D.H.; Ebert, H., Spin-orbit coupling effect in (Ga, Mn) As films: Anisotropic exchange interactions and magnetocrystalline anisotropy, Phys. Rev. B 2011 84 201201. https://doi.org/10.1103/PhysRevB.84.201201
22. Nieves, P.; Arapan, S.; Maudes-Raedo, J.; Marticorena-Sánchez, R.; Del Brío, N.L.; Kovacs, A.; Echevarria-Bonet, C.;Salazar, D.; Weischenberg, J.; Zhang, H.; Vekilova, O.Yu.; Serrano-López, R.; Barandiaran, J.M.; Skokov, K.; Gutfleisch, O.; Eriksson, O.; Herper, H.C.; Schrefl, T.; Cuesta-López, S., Database of novel magnetic materials for high-performance permanent magnet development, Comput. Mat. Sci. 2019 168 188-202. https://doi.org/10.1016/j.commatsci.2019.06.007